# Analysis of Configurational Effects on Hindered Convection of Nonspherical Bacteria and Viruses across Microfiltration Membranes

**ARTICLE** *in* INDUSTRIAL & ENGINEERING CHEMISTRY RESEARCH · OCTOBER 2009

Impact Factor: 2.59 · DOI: 10.1021/ie800579e



**4 AUTHORS**, INCLUDING:

Appala Raju Badireddy
University of Vermont
**37** PUBLICATIONS **952** CITATIONS

SEE PROFILE

Shankar Chellam
Texas A&M University
**107** PUBLICATIONS **2,319** CITATIONS

SEE PROFILE

# Analysis of Configurational Effects on Hindered Convection of Nonspherical Bacteria and Viruses across Microfiltration Membranes

**Ruth E. Baltus,*,† Appala Raju Badireddy,‡ Wendong Xu,‡ and Shankararaman Chellam‡,§**

*Department of Chemical and Biomolecular Engineering, Clarkson University, Potsdam, New York 13699-5705, Department of Civil and Environmental Engineering, University of Houston, Houston, Texas 77204-4003, and Department of Chemical and Biomolecular Engineering, University of Houston, Houston, Texas 77204-4004*

Short-term microfiltration experiments were performed to measure the removal of two gram-negative bacteria (*Brevundimonas diminuta* and *Serratia marcescens*), two bacterial viruses (PRD1 and T4), and several spherical silica particles in a stirred cell under convection-dominated conditions before the onset of fouling. These (bio)colloids ranged from being spherical- to rod-shaped, with an aspect ratio in the range of 1−9. Experimental measurements of the removal of spherical silica and spherical PRD1 bacteriophages were in good agreement with theoretical predictions. A comparison of experimental results for the removal of rod-shaped microorganisms to predictions from a previously developed hindered transport model for capsule-shaped particles indicates shear alignment of the rod-shaped particles within the membrane pore, with microbial passage biased toward an "end on" configuration. Results show that, under the conditions of our measurements, microorganism removal by membranes can be conservatively estimated using the rod diameter as the size parameter in hindered convection predictions.

## 1. Introduction

Microfiltration (MF) and ultrafiltration (UF) membranes are increasingly employed in the food processing, biotechnology, and pharmaceutical industries, for water and wastewater treatment, etc.[1−3] Preventing microbial contamination of the filtered water (physical disinfection and sterile filtration) is integral to these applications.[4,5] To date, several studies have empirically demonstrated the incomplete rejection of bacteria and viruses by microfilters.[6−10] However, quantitative analyses of colloid passage across MF membranes have predominantly focused on spherical colloids, e.g., see refs 11−14, primarily because they are easily available commercially. In contrast, well-defined nonspherical shapes are more difficult to synthesize reproducibly in the laboratory or purchase commercially. Consequently, a fundamental quantitative analysis of the removal of nonspherical colloids by membranes has not yet been performed. In addition, theoretical analyses of colloidal transport have focused primarily on spherical particles. Because of the complexity of the problem, analyses of the rejection of nonspherical particles have been limited to consideration of configurational effects alone. The problem is an important one because rod-shaped bacteria and nonspherical viruses are frequently encountered in membrane feed waters. Their removal from drinking water supplies is essential to providing biologically stable tap water, from wastewater before discharging to receiving water bodies, and to produce water free of viruses, cells, and cell debris during downstream processing.

Studies of colloid and bacterial transport in packed beds have indicated that particle or cell shape is an important parameter in retention. Salerno et al.[15] demonstrated a considerable increase in particle retention within a packed column with increasing particle aspect ratio (=length/diameter) using rodlike polystyrene latex particles with aspect ratios of 2 and 3. In another study of bacterial transport through a packed sand column, Weiss et al.[16] report a chromatographic effect, with changes in the aspect ratio of some bacterial strains as they pass from the inlet to the effluent. Because of the complex geometry in these packed beds, it is difficult to interpret results from these studies using fundamental transport theories that incorporate particle shape effects.

Anderson[17] theoretically examined the transport of rigid nonspherical solutes across porous membranes by considering configurational effects for rodlike particles in cylindrical pores. The reflection coefficient for a rod-shaped particle was predicted to be larger (higher removal) than for a spherical particle with equivalent volume. Experimental results with rodlike tobacco mosaic virus generally agreed with predictions from this theory, when corrections were made to consider polydispersity of virus lengths.[18]

Prud'homme and co-workers[19] compared the elution characteristics of rodlike xanthan polysaccharide and latex spheres in hydrodynamic chromatography measurements performed in a column packed with nonporous spheres. Results indicated that the rodlike xanthan is oriented by the flow field in the chromatography column, eluting from the column with an equivalent volume lying between the volume of a freely tumbling rod and that of a rod which is completely aligned along a streamline. Order of magnitude calculations of the orientational distribution of a rigid dumbbell in unbounded shear flow and in unbounded elongational flow were generally consistent with experimental observations.[20]

While the importance of particle shape on membrane or packed bed transport is generally recognized, detailed information on the removal of nonspherical colloids is still lacking. The principal objective of this research was to quantitatively investigate the role of microorganism aspect ratio on their removal. The passage of rod-shaped bacteria, *Brevundimonas* (formerly *Pseudomonas*) *diminuta* (*B. diminuta*) and *Serratia marcescens* (*S. marcescens*), two bacterial viruses (PRD1 and T4), and spherical silica colloids across clean track-etched membranes is quantitatively interpreted using a previously

* To whom correspondence should be addressed. Tel.: 315-268-2368. Fax: 315-268-6654. E-mail: baltus@clarkson.edu.

† Clarkson University.

‡ Department of Civil and Environmental Engineering, University of Houston.

§ Department of Chemical and Biomolecular Engineering, University of Houston.

10.1021/ie800579e CCC: $40.75 
Published on Web 10/24/2008

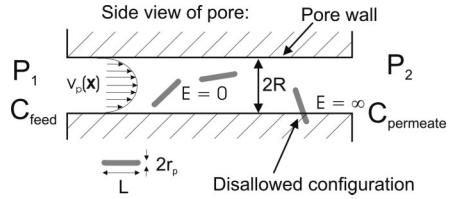


**Figure 1.** Schematic diagram of convective transport of a rod-shaped particle in a cylindrical pore. For spherical particles, $L = 2r_p$.

developed hindered transport theory[17] to draw inferences on microbial orientation as they permeate through the membrane pores.

## 2. Theoretical Work

**2.1. Reflection Coefficient.** The reflection coefficient for filtration, $\sigma$, characterizes solute rejection by a porous membrane. Here, we consider the geometry illustrated in Figure 1, which depicts a long cylindrical capillary pore with radius $R$. The solute particle is either spherical with radius $r_p$ or capsule-shaped with length $L$ and radius $r_p$ and the solvent is treated as a continuum. The relative contribution of axial convection and diffusion to particle transport is characterized using the Peclet number, $Pe_L$, which is defined with the pore length as the characteristic length scale. When solute transport is governed by convection ($Pe_L \gg 1$), $\sigma$ is defined by

$$N_s = (1 - \sigma) J_v C_{feed} \tag{1}$$

where $N_s$ is the solute flux across the membrane, $J_v$ is the volume flux (velocity) across the membrane, and $C_{feed}$ is the solute concentration in the bulk feed solution. It is helpful to note that the limit $\sigma = 0$ refers to complete permeation (no rejection) and the limit $\sigma = 1$ refers to complete rejection.

The reflection coefficient is dependent upon hydrodynamic interactions between the particle and the pore wall as well as by steric restrictions that limit the possible positions and orientations of the particle within the pore. These are included in this general expression for $\sigma$:

$$\sigma = 1 - \frac{\int\int G(\mathbf{x}, \boldsymbol{\psi})\, v_p(\mathbf{x}) \exp(-(E(\mathbf{x}, \boldsymbol{\psi})/kT))\, d\mathbf{x}\, d\boldsymbol{\psi}}{\int\int v_p(\mathbf{x})\, d\mathbf{x}\, d\boldsymbol{\psi}} \tag{2}$$

where $G(\mathbf{x},\boldsymbol{\psi})$ is the lag coefficient (velocity of the particle at position $\mathbf{x}$ and orientation $\boldsymbol{\psi}$ relative to the fluid velocity at $\mathbf{x}$ if the particle was not present) which accounts for hydrodynamic interactions, $v_p(\mathbf{x})$ is the fluid velocity in the pore in the absence of any particles, and the interaction energy between solute particle and pore wall is $E(\mathbf{x},\boldsymbol{\psi})$. Dilute solutions, where particle−particle interactions are negligible, are assumed.

**2.2. Spherical Particles.** Theoretical efforts to describe particle transport in pores of comparable dimensions have focused primarily on developing relationships for $G(\mathbf{x},\boldsymbol{\psi})$ as well as the analogous hindrance factor for diffusion. Early results were summarized in a review article by Deen.[13] More recently, Dechadilok and Deen[21] provided an updated review that includes more accurate expressions for both convective and diffusive hindrance factors, but only for spherical particles (where particle orientation is not a factor).

We will limit our discussion here to results developed by considering only steric particle−pore wall interactions. In the absence of any long-range interactions, the interaction energy $E$ is equal to either 0 or ∞, depending upon whether the particle position results in intersection of the particle with the pore wall ($E = \infty$) or not ($E = 0$). Bungay and Brenner[12] developed a centerline approximation for $G$ which is valid for all relative particle sizes. Brenner and Gaydos[22] used matched asymptotic expansions to derive an expression for $G(x)$ that is valid for particles with size < ∼10% of the pore size. Ennis et al.[23] combined these results using a Padé approximation. Upon integrating over the pore cross-sectional area, their result is

$$\sigma = 1 - [1 - \lambda]^2 \left[\frac{1 + 3.867\lambda - 1.907\lambda^2 - 0.834\lambda^3}{1 + 1.867\lambda - 0.741\lambda^2}\right] \tag{3}$$

where $\lambda$ is the ratio of particle to pore size. Higdon and Muldowney[24] performed numerical calculations to determine $G(x)$ for a range of $\lambda$, and Dechadilok and Deen[21] numerically integrated eq 2 with these values to determine $\sigma$ for various $\lambda$. A comparison of this exact numerical result to eq 3 showed excellent agreement. We therefore conclude that eq 3 provides us with an accurate theoretical prediction of the reflection coefficient for rigid spherical particles in cylindrical pores when only steric particle−pore wall interactions are important.

**2.3. Rod-Shaped Particles.** Equation 2 is a general expression which is valid for particles of any shape. However, expressions for the lag coefficient $G(\mathbf{x},\boldsymbol{\psi})$ are not available for nonspherical particles in small pores. Anderson[17] developed an analysis for the convective transport of capsule-shaped particles in cylindrical pores where it was assumed that $G(\mathbf{x},\boldsymbol{\psi}) = 1$. Therefore, the results are based solely on configurational effects, i.e., on consideration of the sterically allowed positions and particle orientations in the pore. Again, only steric particle−pore wall interactions are considered. However, $E$ depends on both radial position as well as particle orientation for nonspherical particles. Results from this analysis for particles with different aspect ratios show that $\sigma$ increases with the aspect ratio for particles with the same dimensionless volume equivalent diameter.

Bhalla and Deen[25] present results from a theoretical analysis of the osmotic reflection coefficient for prolate and oblate spheroids in cylindrical and slit pores. The osmotic reflection coefficient characterizes osmotic driven flow in a pore that separates reservoirs with different solute concentration. This system is different from the situation depicted in Figure 1 for pressure-driven flow, and different theoretical approaches are used to calculate the two reflection coefficients. The differences between the two reflection coefficients have been discussed by a number of investigators.[13,26−28] Levitt used Onsager's reciprocity relationship with a hydrodynamic−thermodynamic analysis to argue that the two coefficients are identical.[28] Others have noted that there are small differences between the two that arise because hydrodynamic solute−pore wall interactions are not included in expressions for the osmotic reflection coefficient.[13,21,26] Bhalla and Deen[25] suggest that the osmotic theory approach may be incomplete. In any event, the differences between the two coefficients are smaller than typical experimental uncertainty. Bhalla and Deen's results for prolate spheroids follow the trends reported by Anderson for rod-shaped solutes, with the reflection coefficient increasing (i.e., a tighter membrane) with increasing particle aspect ratio.

In both Anderson's and Bhalla and Deen's analyses, it is assumed that all sterically allowed particle orientations are equally probable. For nonspherical particles under shear flow with high rotational $Pe$, particles can become aligned with the flow, making orientations along streamlines more probable than other orientations. The shear-induced alignment of nonspherical particles (dumbbells and prolate spheroids) near a plane wall was analyzed by Nitsche and Roy for small rotational $Pe$ conditions.[29] Results showed that, for a spheroid with aspect

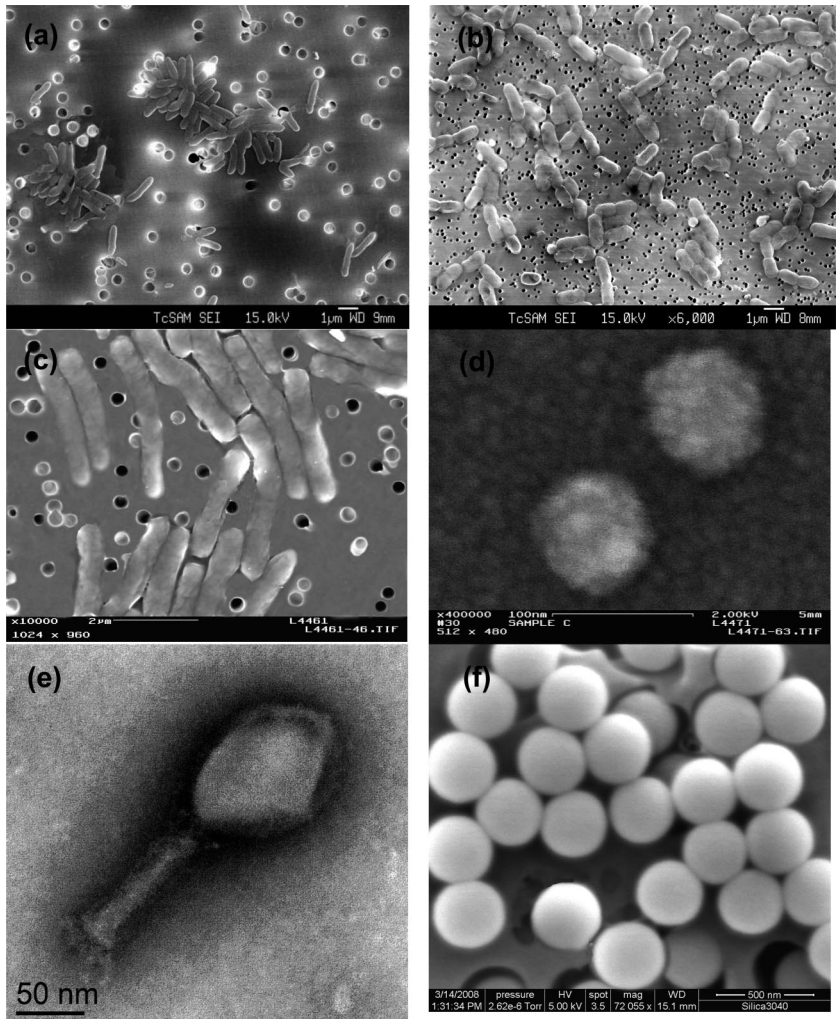


**Figure 2.** Electron micrographs of bacteria *B. diminuta*, *S. marcescens*, and long *B. diminuta*, (a−c respectively), bacteriophages PRD1 and T4 (d and e, respectively), and colloidal silica (f).

ratio = 10, steric and hydrodynamic wall effects altered the distribution of particle orientation (and therefore particle concentration) in the vicinity of the wall by ∼15−20%.

In this paper, we compare experimentally measured reflection coefficient values for rod-shaped bacteria, viruses, and spherical silica particles to values predicted using eq 2 and the approach developed by Anderson.[17] Expressions for $G(\mathbf{x},\psi)$ are not available for nonspherical particles, so we assume $G(\mathbf{x},\psi) = 1$, as did Anderson. The integrals in eq 2 are evaluated by first integrating over the pore cross-sectional area at a fixed particle orientation and then integrating over all possible orientations.

## 3. Experimental Work

**3.1. Bacteria.** *B. diminuta* and *S. marcescens* were used primarily because they are widely used for sterility validation of membranes rated at 0.20 and 0.45 $\mu$m, respectively.[1,30] Bacteria were grown in batch culture using tryptic soy broth at 30 and 26 °C, respectively, harvested by centrifugation at 5000*g* for 10 min at 4 °C, and washed twice by phosphate-buffered saline solution (PBS, pH = 7.3, 137 mM NaCl, 2.7 mM KCl, 4.3 mM $Na_2HPO_4 \cdot 7H_2O$, 1.4 mM $KH_2PO_4$). Bacterial pellets were resuspended in PBS and filtered immediately. More detailed information on bacterial growth procedures can be found in our recent publications.[31,32] Experiments were performed using early stationary phase cultures to avoid any net change in feed bacterial concentration (to accurately calculate rejection) and to reduce pore clogging by autolytic cellular debris.[33] Scanning electron micrographs of at least 45 cell images revealed that *B. diminuta* had a diameter of 0.39 ± 0.03 $\mu$m and length of 1.54 ± 0.27 $\mu$m, resulting in an aspect ratio of ∼4 that is in the range reported earlier.[30,33] (The value before the ± sign is the average, and the value after it is the standard deviation.) *S. marcescens* was 0.65 ± 0.10 $\mu$m in diameter and 2.21 ± 0.43 $\mu$m in length (aspect ratio = 3.4).

Experiments were also performed using *B. diminuta* harvested after incubation for an extended period to increase their aspect ratio. *B. diminuta* were first batch-cultured by transferring a colony of bacteria to 10 mL of tryptic soy broth and incubated overnight. Next, 0.1 mL of the overnight culture was spiked into 25 mL of tryptic soy broth, incubated for an extended period (∼48 h) followed by centrifugation, washing, and resuspension in the PBS as mentioned above. The bacterial suspension in PBS was kept at room temperature overnight prior to filtration. Under these conditions, the average length of *B. diminuta* increased to 3.57 ± 0.82 $\mu$m, while the diameter remained approximately constant at 0.40 ± 0.08 $\mu$m (aspect ratio = 8.9). It is likely that bacteria remained attached even after internal division (cell division rate lower than cell mass increase rate) resulting in longer rods.[34]

Electron micrographs of bacteria, viruses (see section 3.2), and colloidal silica (see section 3.3) employed in this research are shown in Figure 2. Prior to imaging by scanning electron

microscopy, bacteria were fixed on a membrane surface using 2.5% glutaraldehyde at 4 °C overnight. Following fixation, the samples were gently washed with ultrapure water, sequentially dehydrated using graded ethanol (50, 75, 90, 95, and 100% (v/v)) and sputter-coated with gold atoms to a thickness of ~10 nm. Such a procedure has been shown to closely preserve the bacterial cell size and shape and thus maintains the original morphology of the cell.[35]

**3.2. Viruses.** Two bacteriophages PRD1 and T4 were used as model viruses. Bacteriophages are used without loss of generality[36] because they are similar to animal viruses but avoid the need for animal cell lines, biohazards to humans, animals, or the environment, and potential difficulties in obtaining reliable and reproducible results and have been frequently used in previous environmental investigations; e.g., see refs 6, 7, 37, and 38. The polyvalent phage PRD1 was nearly spherical with a diameter of 80 ± 3 nm under our growth conditions (Figure 2d) and has double icosahedral capsids with an internal lipid layer.[39] PRD1 typifies medium-sized DNA viruses in the approximate size range of ~60−80 nm such as adenovirus and rotavirus. T4 has six contractile tail fibers, a head (118 × 86 nm), and a tail (118 × 24 nm) as seen in Figure 2e. We define the aspect ratio for T4 to be the ratio of the total length (236 nm) to the head diameter, yielding a value of 2.7. The fibrous proteins are used to recognize their host receptors similar to adenoviruses and reoviruses. The genome of both viruses is comprised of linear double-stranded DNA.[39,40]

The double-top agar layer plaque technique was employed for assaying both bacteriophages. An initial PRD1 stock was obtained from David Metge's laboratory (United States Geological Survey, Boulder, CO) and propagated using *Salmonella typhimurium* (*S. typhimurium*) LT2 (ATCC 19585) as the host bacterium. *S. typhimurium* were first cultured for 18−24 h in tryptic soy broth (TSB; Difco, Detroit, MI) and later transferred to fresh TSB and grown to midlog phase for 3−6 h at 37 °C. Stock PRD1 was initially diluted in the same PBS that was used in bacterial filtration experiments to a target concentration of ~$10^6$ PFU/mL. Next, *S. typhimurium* suspension (0.9 mL) and phage dilution (0.1 mL) were mixed in 3 mL of soft overlay agar and poured on to presolidified tryptic soy agar (TSA, 1.5% agar; Difco) Petri dishes. Sterile PBS (6 mL) was then added to Petri dishes that resulted in confluent plaques to extract viruses into the buffer after incubation for 24 h at 37 °C. The PBS solution containing PRD1 phages was decanted and centrifuged at 5000*g* for 10 min to remove bacterial debris. Additional purification of fresh PRD1 was achieved by filtering the supernatant through a track-etched membrane rated at 0.2 μm (PCTE Nucleopore Inc., Pleasanton, CA) and then ultracentrifuging the filtrate (Beckman LB-70) at 100000*g* for 2 h. The phage pellet was resuspended in PBS and stored at 4 °C. A similar procedure was used to prepare and enumerate the T4 phage (ATCC 11303-B4) except its host was *Escherichia coli* (*E. coli*) (ATCC 11303). Fresh phage stock was prepared immediately preceding each experiment.

Experimental samples of the microfiltered water were serially diluted before preparing triplicate plates. For accurate enumeration of permeate phage concentration, only plates having 30−300 plaques were counted.[41] Counting was performed manually using a Scienceware colony counter (Bel-Art Products, Pequannock, NJ).

**3.3. Colloidal Silica.** Three colloidal silica (MP4540, MP3040, and MP2040, Nissan Chemical Industries Ltd., Houston, TX), with respective diameters of 0.455 ± 0.013, 0.322 ± 0.014, and 0.194 ± 0.01 μm, were employed. As seen in Figure 2f (MP3040) and in Chellam and Xu[31] (MP4540), these colloids were spherical and nearly monodispersed. Within the limits of the SEM imaging, the aspect ratio of these particles was 1. Silica concentration was measured using light extinction at 600 nm using a 5 cm path length cell (DR-6000, Hach Co., Loveland, CO). Highly linear calibration curves ($R^2$ > 0.997) were obtained for silica concentrations in the range of 1−250 mg/L. Using a feed concentration ~ 100 mg/L and a high path length increased the sensitivity necessary to measure low permeate concentrations.

**3.4. Membranes.** Hydrophilic track-etched membranes (Isopore, Millipore Corp., Bedford, MA) of varying rated pore diameters (0.1, 0.2, 0.4, 0.6, 0.8, 1.0, 1.2, and 5.0 μm) were employed because they possess nearly cylindrical pores facilitating the application of hydrodynamic hindered transport models to quantify (bio)colloidal transport. Pore sizes were measured using three different techniques. Digital image analysis of electron micrographs of the membrane surface were obtained using a field emission scanning electron microscope (FE-SEM, JSM-6330F, JEOL, Peabody, MA) and the procedure described recently by us.[42] Briefly, a commercially available program (SCION IMAGE, Frederick, MD) was used to convert the SEM image into a binary color image so that filter pores were displayed in black with a white background. Next, the area of each pore was calculated by counting the number of contiguous black pixels that enveloped a continuous region. The pixel size was calibrated using the scale bar in the image, and the pore diameter was calculated assuming a cylindrical cross-section. A minimum of 180 pores of at least five separate SEM images were measured to obtain a representative value.

Membrane pore size distributions were also measured by gas−liquid porosimetry (Porometer III, Beckman Coulter, Miami, FL). A proprietary fluorinated hydrocarbon (Porofil) having low surface tension and low vapor pressure was employed. Additional information on the theoretical background and limitations of this technique can be found elsewhere.[3]

Average pore sizes were also determined from hydraulic permeability measurements. The pure water flux of membranes employed was measured in the pressure range of 5−25 psig with ultrapure water produced from a commercial laboratory-scale system (Max159 Modulab, U.S. Filter Corp., Lowell, MA). The system consisted of multistaged treatment with granular activated carbon, mixed bed ion exchange, reverse osmosis, and ultraviolet irradiation and consistently produced ultrapure water with 18.00 MΩ·cm resistivity and dissolved organic carbon concentration > 3 μg/L. The effective pore diameter based on hydraulic permeability was calculated from the experimental water flux and average porosity obtained from electron microscopy. Pore densities were measured by digital image analysis of electron micrographs of the membrane surface. At least five separate images of random areas of each membrane were analyzed using an image analysis program (SCION IMAGE) as described in our earlier publication.[42]

**3.5. Filtration Procedure.** Constant-pressure, stirred microfiltration experiments were performed at room temperature using a commercially available cell (model 8010, Millipore) with an effective membrane area of 4.1 $cm^2$. A computerized data acquisition system (LabVIEW, National Instruments, Austin, TX) was employed to monitor the pressure by an analog pressure transducer (PX303-050G5V, Omega Engineering Co., Stamford, CT) and the cumulative permeate mass by a digital weighing balance (Ohaus Navigator N1H110, Fisher Scientific, Houston, TX). The hold-up volume of this system was kept at a minimum value by decreasing the length of all tubing and the number of

**Table 1. Feed Concentrations of Colloidal Particle Systems Used for Membrane Rejection Measurements[a]**

| colloid | concentration | volume fraction |
|---|---|---|
| *B. diminuta* | $O(10^8)$ CFU/mL | $O(10^{-5})$ |
| *B. diminuta* long | $O(10^8)$ CFU/mL | $O(10^{-4})$ |
| *S. marcescens* | $O(10^8)$ CFU/mL | $O(10^{-4})$ |
| PRD1 | $O(10^6)$ PFU/mL | $O(10^{-10})$ |
| T4 | $O(10^6)$ PFU/mL | $O(10^{-10})$ |
| silica | $O(10^2)$ mg/L | $O(10^{-5})$ |

[a] CFU = colony forming units; PFU = plaque forming units.

fittings in order to accurately measure membrane rejection. More detailed information on the apparatus can be obtained from our recent publications.[31,32]

To decrease electrostatic interactions between (bio)colloids and membrane pores while simultaneously maintaining microorganism viability, all filtration experiments were conducted with the high ionic strength PBS, pH =7.3 (400 mM prepared by adding NaCl to 1 × buffer) serving as the background. Before filtering microorganisms and colloidal silica, 250 mL of the PBS buffer solution was passed through the apparatus to fully wet the membrane and wash it of any chemicals used for preservation. Any remaining buffer in the apparatus was carefully drained prior to filtering colloids to avoid dilution artifacts during sampling and permeate concentration measurement. Particle concentrations in the feed solution are provided in Table 1.

The suspension immediately above the membrane was kept vigorously stirred at 3000 rpm using a magnetic Teflon rod to minimize concentration polarization and fouling. Individual experiments were terminated before any fouling could be discerned. Hence, the reflection coefficient, $\sigma$, was calculated as

$$\sigma = 1 - \frac{C_{\text{permeate}}}{C_{\text{feed}}} \tag{4}$$

Experiments were conducted at room temperature in the pressure range of 5−25 psig for various pore sizes, corresponding to high $Pe_L$ so that diffusional transport in the axial direction can be assumed to be negligible.[13] Permeate samples were collected after filtering ~5−10 mL to measure rejection.

Viable counts of *B. diminuta* and *S. marcescens* in the feed tank did not change within 5 h under feed pressures of 0 and 25 psig. Viable concentrations in the permeate and feed waters were statistically identical when bacteria were passed through a membrane with rated pore size much larger than bacteria sizes (nominal pore size = 5 $\mu$m) at a pressure of 10 psig. Another experiment was performed where the PRD1 virus was kept in contact with a 1 $\mu$m membrane with a background electrolyte concentration of 400 mM (the same as that used in the filtration experiments). Aqueous PRD1 concentrations remained constant over a 2 h period, demonstrating no loss of bacterial infectivity and no adsorptive losses on the membrane. In summary, these controls demonstrate that under our experimental conditions (1) viable concentrations of bacteria and viruses did not change during experimentation and (2) there were no significant adsorptive losses of bacteria and viruses on the feed tank surfaces, tubes, fittings, and the membranes. Hence, any decreases in microorganism concentrations in the permeate was attributed solely to membrane rejection.

## 4. Results and Discussion

**4.1. Membrane Pore Sizes.** Average pore sizes along with the standard deviations for the particular batch of membranes employed in this study obtained by digital image analysis of electron micrographs, porosimetry, and hydraulic permeability measurements are given in Table 2.

As reported earlier,[1,3,42−44] differences were observed between the nominal values reported by the manufacturer and those measured by us. Since the track-etch polycarbonate membranes are negatively charged at pH 7.3,[45,46] the possibility that counter-electroosmosis influenced the pure water permeability measurements was considered. Counter-electroosmosis is the electroosmotic flow resulting from the induced streaming potential that arises because positive and negative ions partition differently into a charged pore and therefore have different convective fluxes in the pore. In order for the system to maintain electrical neutrality, an electrophoretic ion flux results which is in the opposite direction in the pore to the convective driven flux. If counter-electroosmosis is important, one might expect pore sizes determined from hydraulic permeability measurements to yield pore sizes smaller than the true size because the pressure driven flow will be countered by an electroosmotic driven flow. Saksena and Zydney[47] show that the magnitude of electroosmotic flow increases with decreases in solvent ionic strength and with decreases in pore size. All hydraulic permeability measurements were performed with pure, low ionic strength water. If counter-electroosmosis were important for our systems, one would expect it to impact measurements with the small pore membranes to a greater extent than the larger pore membranes. A comparison of the pore sizes determined from porosimetry to those determined from hydraulic permeability shows, in general, better agreement between the two measurements with the small pore membranes than for the larger pore membranes. Therefore, it appears unlikely that counter-electroosmosis provides the explanation for the relatively smaller effective pore sizes observed with the hydraulic permeability measurements when compared to the porosimetry measurements. The observed differences between pore size values determined using the three different techniques are discussed later in this paper with our discussion of the results from silica particle rejection measurements.

**4.2. Reflection Coefficients for Colloidal Silica Particles.** Measured reflection coefficients for the spherical silica particles are presented in Figure 3 as a plot of $\sigma$ versus dimensionless particle size ($r_p/R$). Results are presented using membrane pore sizes determined by SEM, porosimetry, and hydraulic permeability measurements. With the range of particle and pore sizes used in these experiments, we were able to collect data over a wide range of dimensionless particle sizes, with $\sigma$ values ranging from 0.2 to 1.0. Experimental results are compared to reflection coefficient values predicted for spherical particles using eq 3 (which incorporates hydrodynamic interactions) as well for the case when only steric interactions are considered (i.e., $G = 1$ for all particle positions). For the same dimensionless particle size, the reflection coefficient is predicted to be slightly larger when hydrodynamic effects are included. However, the difference between the two theoretical approaches is quite small. Measured values were in very good agreement with the theoretical predictions, confirming the validity of the pore size values and in the experimental procedures used for the rejection measurements.

The good agreement between theory and experiment also confirms the assumption that only steric particle−pore wall interactions are governing particle transport in these systems. The agreement between experiment and theory for the silica particles also confirms our assumption that any concentration polarization at the membrane surface is insignificant. Additional support for this assumption is found by recognizing that the resistance to flow provided by the membrane depends

**Table 2. Characteristics of Membranes Used in This Study**[a]

| nominal pore size (nm) | membrane thickness ($\mu$m) | pore density (no./m$^2$) | pore diameter by SEM (nm) | pore diameter by porosimetry (nm) | pore diameter by hydraulic permeability (nm) |
|---|---|---|---|---|---|
| 100 | 10 | $4.67 \times 10^{12}$ | $113 \pm 8$ | $173 \pm 6$ | 138 |
| 200 | 10 | $4.35 \times 10^{12}$ | $158 \pm 23$ | $361 \pm 12$ | 225 |
| 400 | 10 | $7.90 \times 10^{11}$ | $424 \pm 96$ | $589 \pm 20$ | 470 |
| 600 | 9 | $3.65 \times 10^{11}$ | $498 \pm 54$ | $649 \pm 21$ | 492 |
| 800 | 9 | $3.59 \times 10^{11}$ | $642 \pm 53$ | $872 \pm 32$ | 651 |
| 1000 | 10 | $2.38 \times 10^{11}$ | $946 \pm 56$ | $1287 \pm 62$ | 688 |
| 1200 | 9 | $1.85 \times 10^{11}$ | $1048 \pm 120$ | $1298 \pm 54$ | 844 |
| 5000 | 8 | $3.60 \times 10^{9}$ | $3821 \pm 421$ | $4590 \pm 230$ | 2419 |

[a] Membrane thickness values are reported by the manufacturer. All other parameters were experimentally determined as part of this work.

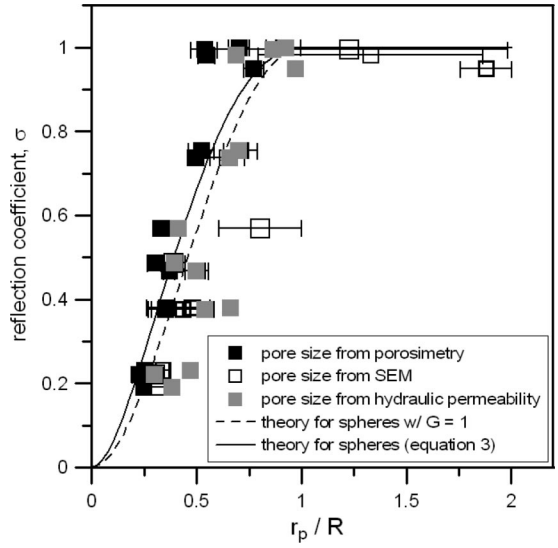


**Figure 3.** Experimental results for spherical silica colloids.

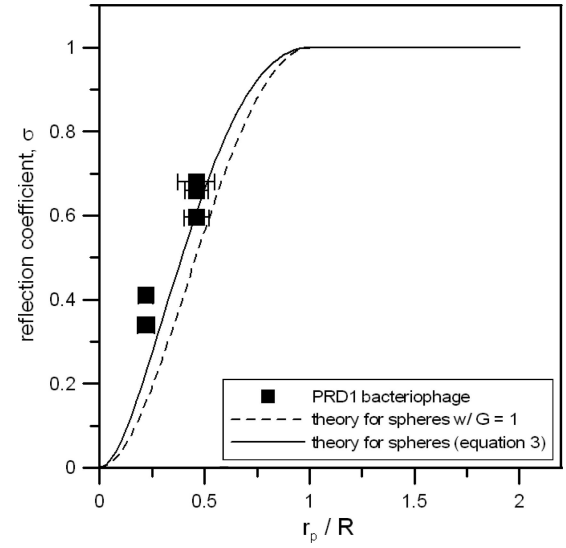


**Figure 4.** Experimental results for PRD1 bacteriophage. Pore sizes determined by porosimetry were used to nondimensionalize PRD1 size.

upon the membrane pore size as well as the transmembrane pressure used during filtration. Therefore, the relative contribution of any concentration polarization layer to the overall resistance to transport is expected to vary with membrane pore size as well as with the feed pressure established during the filtration experiments. The results presented in Figure 3 were obtained with experiments performed over a range of transmembrane pressures and with different pore size membranes. The fact that excellent agreement between theory and experiment is seen for the entire data set supports the assumption that there is no significant external membrane resistance for these systems.

A statistical comparison between measured reflection coefficients and theoretical predictions indicates the best agreement between theory and experiment is found when the pore size determined using porosimetry is used for nondimensional particle size. Uncertainties in pore sizes determined with SEM may arise because SEM images only provide information about the membrane surface and those images can potentially be distorted because of the conductive metal coating needed to image the polymer film. In addition, imaging is done in a vacuum under dehydrated conditions whereas porosimetry measures an effective diameter of the entire pore using a fully wetting liquid.[3,48] Uncertainties in pore sizes determined using hydraulic permeability may arise because of uncertainties in membrane thickness/pore length as well as in pore density determinations. Analogous differences between pore diameters measured using different techniques have been previously reported.[1,3,43,44] In the analyses that follow, we use the pore size determined from porosimetry when comparing experimental measurements to theoretical predictions.

**4.3. Reflection Coefficients for PRD1 Bacteriophage.** Measured reflection coefficients for PRD1 bacteriophage particles are presented in Figure 4, where again measured values are compared to theoretical predictions for spherical particles. These measurements were only made with two different pore size membranes, limiting the range of measured reflection coefficient values. As observed with the silica particles, agreement between measured and predicted values is quite good. The fact that measured reflection coefficient values for these bacteriophage particles follows the theoretical prediction developed for rigid spherical particles indicates that the conformation of these particles is not altered to any significant extent during transport through the confined space within the pores, demonstrating that PRD1 behaves as a rigid sphere during microfiltration.

**4.4. Reflection Coefficients for Rod-Shaped Bacteria.** Experimental results collected with the two different *B. diminuta* bacteria and with *S. marcescens* are presented in Figure 5a as a plot of measured reflection coefficient versus dimensionless size. The particle size used to prepare this plot is the diameter of a sphere with volume equivalent to that of the rod-shaped particle. Included in this plot are the theoretical predictions for spherical particles and for rod-shaped particles with aspect ratios of 2, 4, and 10. Here, the prediction for spheres includes hydrodynamic interactions (eq 3), but the theory for rods only considers configurational effects. This explains the overlap between the prediction for spheres and for rods with an aspect ratio of 2. For a given dimensionless particle size, theoretical calculations predict that the reflection coefficient increases with the aspect ratio. The experimental results presented in Figure 5a do not follow this trend, with reflection coefficients for these

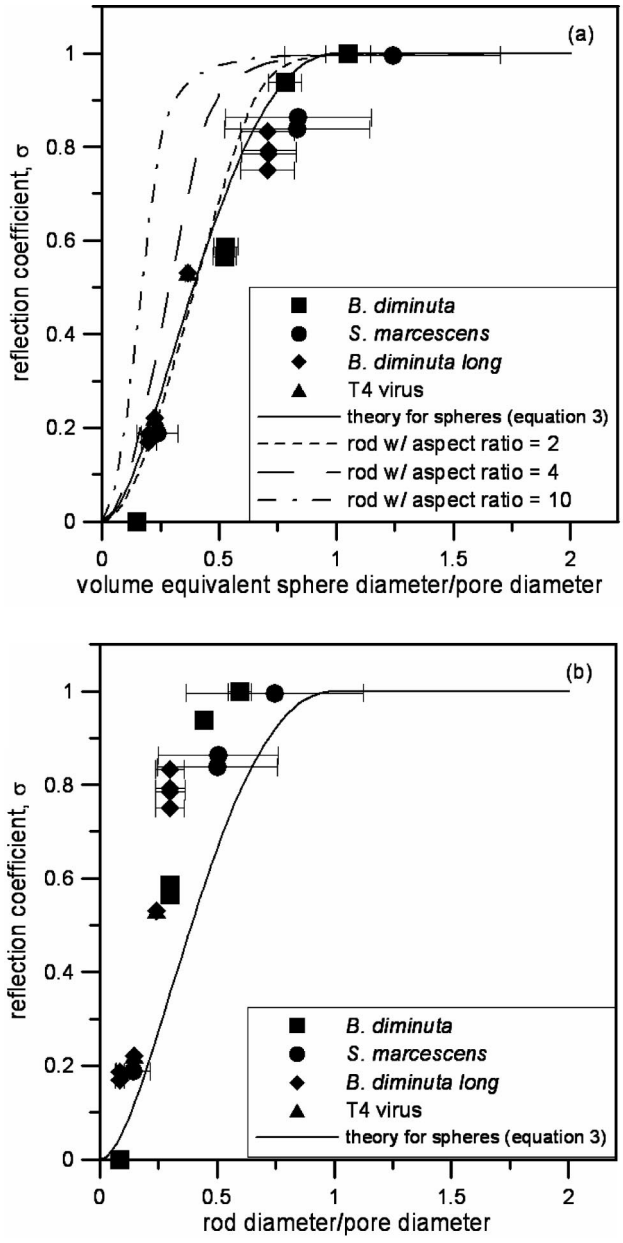


**Figure 5.** Comparison of experimental results for rod-shaped microorganisms with theoretical predictions. The aspect ratio of *B. diminuta* is 4, of *S. marcescens* is 3.4, and of *B. diminuta* long is 8.9, and that of T4 virus, based on the head diameter and the head plus tail length, is 2.7. In a, results are presented using the volume equivalent sphere diameter to characterize particle size. In b, results are presented using the rod diameter to characterize particle size. Pore sizes determined by porosimetry were used to nondimensionalize microorganism size.

particles following a similar trend, independent of particle aspect ratio. In contrast to theoretical expectations, experimentally measured reflection coefficient values are in general agreement with the theoretical prediction for spherical particles with the same volume.

To interpret the results presented in Figure 5a, it is useful to consider time scales for axial transport (pore length/fluid velocity), for radial diffusion ($R^2/D_{trans}$), and for rotational relaxation ($1/D_{rot.}$). The translational and rotational diffusion coefficients of short rodlike particles depend upon the aspect ratio of the particles:[49]

$$D_{trans} = \frac{kT}{3\pi\eta L}(\ln p + 0.312 + 0.565p^{-1} - 0.100p^{-2}) \quad (5)$$

$$D_{rot.} = \frac{3kT}{\pi\eta L^3}(\ln p - 0.662 + 0.917p^{-1} - 0.050p^{-2}) \quad (6)$$

where $p$ is the particle aspect ratio.

Values for the translational and rotational diffusion coefficients and characteristic times for axial transport, radial diffusion, and rotational relaxation are summarized in Table 3. Values were calculated for two experiments with different membrane pore sizes and different transmembrane pressures, providing the maximum and minimum characteristic time values.

For all measurements, the residence time for axial transport was $\sim 10^{-5}-10^{-3}$ s, depending on the membrane pore size and the transmembrane pressure. Radial diffusion times were $\sim 10^{-9}-10^{-7}$ s, and rotational relaxation times ranged from $\sim 10^{-3}$ to 10 s. In all cases, the axial residence time was considerably larger than the characteristic time for radial diffusion. Therefore, the assumption that particles are able to sample all sterically available radial positions and are not transported through the pore along a limited number of streamlines is valid.

A comparison of the three time scales reveals that the rotational relaxation time is considerably greater than either the axial residence time or the radial diffusion time. The one exception to this trend is for the T4 experiment in the smallest pore membrane where the time scales for rotational relaxation and for axial transport are comparable. In the theoretical development of Anderson,[17] it is assumed that all sterically allowed particle orientations within the pore are equally probable. However, our comparison of relative time scales indicates that the shear rate within the pore may be sufficiently large so that the particles may become aligned with the flow and may not sample all sterically allowed orientations. If the particles pass through the pore with solely an "end on" orientation, the rod diameter becomes the appropriate characteristic particle size parameter and the reflection coefficient is expected to be independent of rod length and aspect ratio. The results presented in Figure 5a follow this trend, with reflection coefficients following a similar trend for particles with different aspect ratios. This explanation is examined further in Figure 5b where the same experimental results are presented, but with the rod diameter rather than the volume equivalent diameter as the particle size parameter. The experimental results are compared to the theoretical prediction for a sphere. When compared in this manner, the reflection coefficients for the rod-shaped bacteria are larger than those predicted for a sphere with the same diameter.

There are two possible explanations for the discrepancy between the predictions for spherical particles and the results presented in Figure 5b. If the rods are able to sample some, but not all, sterically allowed orientations off the pore axis, the particle reflection coefficient would be larger than predicted for a sphere with the same diameter. In other words, the orientation of the rod-shaped particles in the pore may be only biased toward an end on configuration. This explanation is similar to one presented by Prud'homme and Hoagland[20] for the transport of xanthan rods in hydrodynamic chromatography. Hydrodynamic interactions can also provide an explanation for the discrepancy between measured and predicted reflection coefficients in Figure 5b. Agreement between the theoretical prediction for a sphere and the measured reflection coefficients for rods aligned with the flow is expected only if hydrodynamic interactions are neglected. In an unbounded fluid, the resistance experienced by a rod with flow parallel to its long axis is expected to be ~20−200% larger than that of a sphere with

**Table 3. Summary of Translational and Rotational Diffusion Coefficients (in Bulk Solution) and Characteristic Times for Axial Transport, Radial Diffusion, and Rotational Relaxation**

| | | *B. diminuta* | *S. marcescens* | *B. diminuta* long | T4 |
|---|---|---|---|---|---|
| | Particle length ($\mu$m) | 1.54 | 2.21 | 3.57 | 0.236 |
| | Aspect ratio | 4 | 3.4 | 8.9 | 2.7 |
| | $D_{trans} \times 10^{13}$ ($m^2/s$) | 6.02 | 3.91 | 3.58 | 33.0 |
| | $D_{rot.}$ ($s^{-1}$) | 1.00 | 0.30 | 0.14 | 195 |
| | Rotational relaxation time (s) | 1.00 | 3.83 | 7.24 | $5.1 \times 10^{-3}$ |
| 100 nm Nominal Pore Size Membrane with 5 psi Transmembrane Pressure | Axial residence time (s) | $3.1 \times 10^{-3}$ | $3.1 \times 10^{-3}$ | $3.1 \times 10^{-3}$ | $3.1 \times 10^{-3}$ |
| | Radial diffusion time (s) | $1.24 \times 10^{-8}$ | $1.91 \times 10^{-8}$ | $2.09 \times 10^{-8}$ | $2.27 \times 10^{-9}$ |
| 1200 nm nominal Pore Size Membrane with 25 psi Transmembrane Pressure | Axial residence time (s) | $2.1 \times 10^{-5}$ | $2.1 \times 10^{-5}$ | $2.1 \times 10^{-5}$ | $2.1 \times 10^{-5}$ |
| | Radial diffusion time (s) | $6.99 \times 10^{-7}$ | $1.08 \times 10^{-6}$ | $1.18 \times 10^{-6}$ | $1.28 \times 10^{-7}$ |

the same diameter, depending upon the rod length.[50] It should also be added that the difference between theory and observation is expected to increase with the rod aspect ratio, which is not seen with our results.

The discussion above focuses on shear alignment of the rod-shaped particles within the membrane pores. Given the relatively long rotational relaxation times for these systems, it also seems possible that the particles become aligned with the flow in the bulk solution as the fluid enters the pore. Following an analysis presented by Keh,[51] we consider the converging flow in the vicinity of the pore entrance with the pore modeled as a point sink in a plane wall. The important parameter here is the elongation rate which will dominate fluid flow directly outside the pore entrance (incident angle = 0 in Keh's analysis). If we consider the important characteristic length for elongational flow at the pore entrance to be equal to five times the pore radius, the elongation rate = (flow rate through the pore)/$(5R)^3 \sim 10^7$ $s^{-1}$. This elongation rate is considerably larger than the rotational diffusion coefficient of the bacteria particles ($D_{rot.}$ in Table 3). The elongation rate will decrease as one moves from directly outside the pore to the membrane surface near the pore entrance, but the general conclusions from the order of magnitude analysis presented here do not change. This means that the probability that the particles sample all orientations as they are transported from the bulk solution into the pore is quite small. The rejection model assumes the particles sample all sterically allowed orientations in establishing particle concentration inside the pore relative to that in the bulk solution. Intuitively, one can expect that alignment of the particles along the streamlines outside the membrane will increase the intrapore concentration at the pore mouth, relative to the value predicted for short rotational relaxation times. Our experimental results are consistent with this bulk solution alignment, with particle rejection observed to be less than predicted for rod-shaped particles with equally probable orientations.

**4.5. Reflection Coefficients for T4 Bacteriophage.** Experimental reflection coefficient values for the T4 bacteriophage are also included in Figure 5a,b. As shown in Figure 2e, this phage is comprised of a head and a tail with different diameters. To conservatively estimate its volume equivalent radius, it was assumed that T4 was rod-shaped with diameter equal to the head diameter along its entire length. When adding the T4 results to Figure 5b, the head size was used as the characteristic particle diameter. Examination of the results in Figure 5a,b reveals that the measured reflection coefficient values for this asymmetric particle are generally consistent with results observed with the rod-shaped bacteria. The narrower diameter of the tail region does not appear to provide any significant increase in the rotational configurations that are sampled by it inside the pore. These results indicate that the behavior of this uniquely shaped virus is governed by the region with the largest diameter.

## 5. Conclusions

The results presented here indicate that theoretical predictions for the convective transport of rod-shaped bacteria do not accurately describe experimental results for the microorganisms examined in this study. This discrepancy between theory and experiment may be due to the fact that hydrodynamic particle−pore wall interactions are neglected in currently available prediction methodologies. However, our results indicate that particle orientation in the pore may be a more significant issue, with alignment biased toward an end on trajectory. In the future, we plan to perform measurements under a broader range of flow conditions, which should help us to more carefully examine this phenomenon. Our future work will also involve the incorporation of hydrodynamic effects in our theoretical analysis of particle transport as well as an examination of pore entrance effects.

The results presented in Figure 5b show that using the rod diameter as the particle size parameter provides conservative criteria for selection of the required membrane pore size when designing a microbial removal process for water treatment systems. It should be emphasized that experiments reported in this paper were designed to conservatively measure microorganism removal before the initiation of fouling, which has been empirically shown to increase virus removal.[6,52] Additionally, unlike track-etched microfilters employed in this research, low-pressure membranes commonly employed in industrial and municipal applications made by phase inversion consist of a random and tortuous network of pores with a wide distribution of effective diameters. Hence, results reported herein should be cautiously extrapolated to "real-world" systems.

## Acknowledgment

We appreciate David Metge (USGS, Boulder, CO) providing us with the initial PRD1 stock. This research has been funded by a grant to S.C. from the National Science Foundation CAREER program (BES-0134301). The contents do not necessarily reflect the views and policies of the sponsors nor does the mention of trade names or commercial products constitute endorsement or recommendation for use.

## Nomenclature

$C_{feed}$ = particle concentration in feed solution ($g/m^3$)
$C_{permeate}$ = particle concentration in permeate solution ($g/m^3$)
$D_{rot.}$ = rotational diffusivity ($s^{-1}$)
$D_{trans}$ = translation diffusivity ($m^2/s$)
$E$ = interaction energy between particle and pore wall (J/mol)

$G$ = particle lag coefficient in pore
$J_v$ = volume flux (velocity) (m/s)
$k$ = Boltzmann constant ($1.38 \times 10^{-23}$ J/K)
$L$ = particle length ($\mu$m)
$N_s$ = particle flux (g/(s·m$^2$))
$p$ = particle aspect ratio (length/diameter)
$Pe_L$ = Peclet number based on pore length
$r_p$ = particle radius ($\mu$m)
$R$ = pore radius (nm)
$T$ = temperature (K)
$v_p$ = fluid velocity in pore (m/s)
$\mathbf{x}$ = position variable (m)
$\lambda$ = particle size/pore size
$\psi$ = particle orientation variable

## Literature Cited


(1) Cheryan, M. *Ultrafiltration and Microfiltration Handbook*; Technomic Publishing: Lancaster, PA, 1998; p 527.

(2) Mallevialle, J.; Odendaal, P. E.; Wiesner, M. R. *Water Treatment Membrane Processes*; McGraw-Hill: New York, 1996.

(3) Zeman, L. J.; Zydney, A. L. *Microfiltration and Ultrafiltration*; Marcel Dekker: New York, 1996; p 618.

(4) Mi, B.; Marinas, B. J.; Curl, J.; Sethi, S.; Crozes, G. Microbial Passage in Low Pressure Membrane Elements with Compromised Integrity. *Environ. Sci. Technol.* **2005**, *39*, 4270–4279.

(5) Jornitz, M. W.; Meltzer, T. H. *Sterile Filtration: A Practical Approach*; Marcel Dekker: New York, 2001; p 623.

(6) Jacangelo, J. G.; Adham, S. S.; Laine, J. M. Mechanism of Cryptosporidium, Giardia, and MS2 Virus Removal by MF and UF. *J. Am. Water Works Assoc.* **1995**, *87* (10), 107–121.

(7) Madaeni, S. S.; Fane, A. G.; Grohmann, G. S. Virus Removal from Water and Wastewater Using Membranes. *J. Membr. Sci.* **1995**, *102*, 65–75.

(8) Sadr Ghayeni, S. B.; Beatson, P. J.; Fane, A. J.; Schneider, R. P. Bacterial Passage through Microfiltration Membranes in Wastewater Applications. *J. Membr. Sci.* **1999**, *153*, 71–82.

(9) Urase, T.; Yamamoto, K.; Ohgaki, S. Effect of Pore Structure of Membranes and Module Configuration on Virus Retention. *J. Membr. Sci.* **1996**, *115*, 21–29.

(10) Wickramasinghe, S. R.; Kalbufss, B.; Zimmermann, A.; Thom, V.; Reichl, U. Tangential Flow Microfiltration and Ultrafiltration for Human Influenza A Virus Concentration and Purification. *Biotechnol. Bioeng.* **2005**, *92* (2), 199–208.

(11) Anderson, J. L.; Quinn, J. A. Restricted Transport in Small Pores: A Model for Steric Exclusion and Hindered Particle Motion. *Biophys. J.* **1974**, *14*, 130–150.

(12) Bungay, P. M.; Brenner, H. The Motion of a Closely Fitting Sphere in a Fluid-Filled Tube. *Int. J. Multiphase Flow* **1973**, *1*, 25–56.

(13) Deen, W. M. Hindered Transport of Large Molecules in Liquid Filled Pores. *J. AIChE* **1987**, *33* (9), 1409–1425.

(14) Mochizuki, S.; Zydney, A. L. Theoretical Analysis of Pore Size Distribution Effects on Membrane Transport. *J. Membr. Sci.* **1993**, *82*, 211–228.

(15) Salerno, M. B.; Flamm, M.; Logan, B. E.; Velegol, D. Transport of Rodlike Colloids through Packed Beds. *Environ. Sci. Technol.* **2006**, *40*, 6336–6340.

(16) Weiss, T. H.; Mills, A. L.; Hornberger, G. M.; Herman, J. S. Effect of Bacterial Cell Shape on Transport of Bacteria in Porous Media. *Environ. Sci. Technol.* **1995**, *29*, 1737–1740.

(17) Anderson, J. L. Configurational Effect on the Reflection Coefficient for Rigid Solutes in Capillary Pores. *J. Theor. Biol.* **1981**, *90*, 405–426.

(18) Long, T. D.; Jacobs, D. L.; Anderson, J. L. Configurational Effects on Membrane Rejection. *J. Membr. Sci.* **1981**, *9*, 13–27.

(19) Prud′homme, R. K.; Froiman, G.; Hoagland, D. A. Molecular-Size Determination of Xanthan Polysaccharide. *Carbohydr. Res.* **1982**, *106*, 225–233.

(20) Prud′homme, R. K.; Hoagland, D. A. Orientation of Rigid Macromolecules during Hydrodynamic Chromatography Separations. *Sep. Sci. Technol.* **1983**, *18* (2), 121–134.

(21) Dechadilok, P.; Deen, W. M. Hindrance Factors for Diffusion and Convection in Pores. *Ind. Eng. Chem. Res.* **2006**, *45*, 6953–6959.

(22) Brenner, H.; Gaydos, L. J. The Constrained Brownian Movement of Spherical Particles in Cylindrical Pores of Comparable Radius: Models of the Diffusive and Convective Transport of Solute Molecules in Membranes and Porous Media. *J. Colloid Interface Sci.* **1977**, *58*, 312–356.

(23) Ennis, J.; Zhang, H.; Stevens, G.; Perera, J.; Scales, P.; Carnie, S. Mobility of Protein through a Porous Membrane. *J. Membr. Sci.* **1996**, *119*, 47–48.

(24) Higdon, J. J. L.; Muldowney, G. P. Resistance Functions for Spherical Particles, Droplets, and Bubbles in Cylindrical Tubes. *J. Fluid Mech.* **1995**, *298*, 193–210.

(25) Bhalla, G.; Deen, W. M. Effects of Molecular Shape on Osmotic Reflection Coefficients. *J. Membr. Sci.* **2007**, *306*, 116–124.

(26) Adamski, R. P.; Anderson, J. L. Solute Concentration Effect on Osmotic Reflection Coefficient. *Biophys. J.* **1983**, *44*, 79–90.

(27) Anderson, J. L.; Malone, D. M. Mechanism of Osmotic Flow in Porous Membranes. *Biophys. J.* **1974**, *14*, 957–982.

(28) Levitt, D. G. General Continuum Analysis of Transport through Pores. *Biophys. J.* **1975**, *15*, 533–551.

(29) Nitsche, J. M.; Roy, P. Shear-Induced Alignment of Nonspherical Brownian Particles Near Walls. *AIChE J.* **1996**, *42*, 2729–2742.

(30) Waterhouse, S.; Hall, G. M. The Validation of Sterilising Grade Microfiltration Membranes with *Pseudomonas diminuta*: A Review. *J. Membr. Sci.* **1995**, *104*, 1–9.

(31) Chellam, S.; Xu, W. Blocking Laws Analysis of Dead-end, Constant Flux Microfiltration of Compressible Cakes. *J. Colloid Interface Sci.* **2006**, *301* (1), 248–257.

(32) Xu, W.; Chellam, S. Initial Stages of Bacterial Fouling during Dead-end Microfiltration. *Environ. Sci. Technol.* **2005**, *39*, 6470–6476.

(33) Leahy, T. J.; Sullivan, M. J. Validation of Bacterial-Retention Capabilities of Membrane Filters. *Pharm. Technol.* **1978**, *2*, 65–75.

(34) Cooper, S. *Bacterial Growth and Division: Biochemistry and Regulation of Prokaryotic and Eukaryotic Division Cycles*; Academic Press: New York, 1991; p 501.

(35) Dykstra, M. J. *Biological Electron Microscopy*; Plenum Press: New York, 1992; p 360.

(36) Grabow, W. O. K. Bacteriophages: Update on Application as Models for Viruses in Water. *Water SA* **2001**, *27* (2), 251–268.

(37) Ryan, J. N.; Elimelech, M.; Ard, R. A.; Harvey, R. W.; Johnson, P. R. Bacteriophage PRD1 and Silica Colloid Transport and Recovery in an Iron Oxide-Coated Sand Aquifer. *Environ. Sci. Technol.* **1999**, *33*, 63–73.

(38) Matsui, Y.; Matsushita, T.; Sakuma, S.; Gojo, T.; Mamiya, T.; Suzuoki, H.; Inoue, T. Virus Inactivation in Aluminum and Polyaluminum Coagulation. *Environ. Sci. Technol.* **2003**, *37*, 5175–5180.

(39) Martin, C. S.; Burnett, R. M.; de.Haas, F.; Heinkel, R.; Rutten, T.; Fuller, S. D.; Butcher, S. J.; Bamford, D. H. Combined EM/X-ray Imaging Yields a Quasi-Atomic Model of the Adenovirus-Related Bacteriophage PRD1 and Shows Key Capsid and Membrane Interactions. *Structure* **2001**, *9* (10), 917–930.

(40) Mesyanzhinov, V. V. Bacteriophage T4: Structure, Assembly, and Initiation Infection Studied in Three Dimensions. *Adv. Virus Res.* **2004**, *63*, 287–352.

(41) Clesceri, L. S.; Greenberg, A. E.; Eaton, A. D., *Standard Methods for the Examination of Water and Wastewater*, 20th ed.; APHA, AWWA, and WEF: Washington, DC, 1998.

(42) Han, K.; Xu, W.; Ruiz, A.; Ruchhoeft, P.; Chellam, S. Fabrication and Characterization of Polymeric Microfiltration Membranes Using Aperture Array Lithography. *J. Membr. Sci.* **2005**, *249*, 193–206.

(43) Kim, K. J.; Stevens, P. V. Hydraulic and Surface Characteristics of Membranes with Parallel Cylindrical Pores. *J. Membr. Sci.* **1997**, *123*, 303–314.

(44) Calvo, J. I.; Hernandez, A.; Pradanos, P.; Martinez, L.; Bowen, W. R.; Pore Size Distributions in Microporous Membranes, I. I. Bulk Characterization of Track-Etched Filters by Air Porometry and Mercury Porosimetry. *J. Colloid Interface Sci.* **1995**, *176*, 467–478.

(45) Lin, N. P.; Deen, W. M. Charge Effects on the Diffusion of Polystyrene Sulfonate through Porous Membranes. *J. Colloid Interface Sci.* **1992**, *153*, 483–492.

(46) Deen, W. M.; Smith, F. G. I. Hindered Diffusion of Synthetic Polyelectrolytes in Charged Micrporous Membranes. *J. Membr. Sci.* **1982**, *12*, 217–237.

(47) Saksena, S.; Zydney, A. L. Pore Size Distribution Effects on Electrokinetic Phenomena in Semipermeable Membranes. *J. Membr. Sci.* **1995**, *105*, 203–216.

(48) Zeman, L.; Denault, L. Characterization of Microfiltration Membranes by Image Analysis of Electron Micrographs. Part I. Method Development. *J. Membr. Sci.* **1992**, *71*, 221–231.

(49) Elmer, W.; Pecora, R. Rotational and Translational Diffusion of Short Rodlike Molecules in Solution: Oligonucleotides. *J. Chem. Phys.* **1991**, *94*, 2324–2329.

(50) Happel, J.; Brenner, H. *Low Reynolds Number Hydrodynamics*; Noordhoff International Publishing: Leyden, The Netherlands, 1973; p 553.

(51) Keh, H. J. Flow-Dependent Rejection of Polymer Chains from Microporous Membranes. *J. Chin. Inst. Chem. Eng.* **1985**, *16*, 395–398.

(52) Mysore, C. S.; Leparc, J. ; Poussade, Y.; Jacangelo, J. G.; Huffman, D. E. Comparing Microbial Rejection Performances of Low-Pressure Membranes in Potable and Non-Potable Waters. In *Membrane Treatment for Drinking Water & Reuse Applications*; Howe, K. J., Ed.; American Water Works Association: Denver, CO, 2006.

*Received for review* April 10, 2008
*Revised manuscript received* August 23, 2008
*Accepted* August 28, 2008

IE800579E